SOILS AND FOUNDATIONS Vol. 48, No. 6, 791–804, Dec. 2008
Japanese Geotechnical Society

# EXPERIMENTS AND PREDICTIONS OF SOIL DESATURATION BY AIR-INJECTION TECHNIQUE AND THE IMPLICATIONS MEDIATED BY MULTIPHASE FLOW SIMULATION

HIDEAKI YASUHARA[i], MITSU OKAMURA[i] and YOSHINORI KOCHI[ii]

## ABSTRACT

Measures preventing an earthquake-induced soil liquefaction are of significant importance to mitigate the liquefaction hazards. An air-injection technique may be a simple, inexpensive method - this leads the saturated soils to the desaturated by injecting pressurized air, resulting in a higher liquefaction strength and lower susceptibility. The objective of this study is to investigate the evolution of desaturation process during air injection into saturated soil deposits and verify the validity of a multiphase flow simulator if it is capable of being applied for predicting the process as well as the distribution of degree of saturation after the air injection ceased. In this study simplified model tests that simulate the air injection into saturated soils using air-injection probes, are conducted using two different sizes of soil containers. The experiments using the small container are aimed to examine the nominal rates and magnitudes of the soil desaturation driven by air injection, whilst those with the large container are performed to obtain not only the rates and magnitudes but also the distributions of the desaturated zones within the soil. The results obtained indicate, although clearly depending on the physical properties of targeted soils, that the evolution of desaturation is strongly controlled by the air pressures injected and the soil permeabilities. Numerical analyses are also conducted using a multiphase flow simulator to describe the evolution of the soil desaturation, and to examine the applicability of the model as a prediction tool enabling an evolution of desaturation *in situ* to be followed with time and space. Predictions show a relatively good agreement with the experimental measurements regarding the rates, magnitudes, and distribution of desaturation specifically for the small-container experiments although predictions of desaturated domain slightly overestimate the measurements for the large-container experiments. Thus, this study indicates that the numerical model described is applicable to field problems when the soil properties in terms of flow transport are well-constrained.

**Key words:** air, liquefaction, laboratory test, numerical analysis, permeability, saturation (**IGC**: D4/E7)

## INTRODUCTION

Measures preventing an earthquake-induced soil liquefaction are of significant importance to mitigate the liquefaction hazards. Improving the strength, density, and drainage characteristics of the soils is one of the most popular methods to reduce the liquefaction susceptibility. For instance, dynamic compaction, compaction grouting, solidification, and drainage techniques are widely applied for the purpose, but their installation costs are generically expensive.

An air-injection technique (Okamura and Teraoka, 2005) may be a simple, inexpensive alternative–this leads the saturated soils to the desaturated by injecting pressurized air, resulting in a higher liquefaction strength and the lower susceptibility. As experimental evidences of lowering liquefaction susceptibility induced by desaturation, Okamura and Teraoka (2005), Yegian et al. (2007) and Takemura et al. (2009) carried out 1g and centrifuge shaking table tests and showed that desaturation of foundation soil has significant effects to reduce generation of excess pore pressure and settlement of structures. Yoshimi et al. (1989) have conducted cyclic torsional shear tests and concluded that a soil specimen shows threefold liquefaction resistance ratio as the degree of saturation decreases from fully-saturated to 70%. Okamura and Soga (2006) derived influential factors of the liquefaction resistance of a partially saturated sand from theoretical consideration and effects of the factors are examined through a series of triaxial tests. They found a unique relationship between the ratio of liquefaction resistance ratio of partially saturated sand to that saturated and the potential volumetric strain. This relationship enables the estimation of the liquefaction resistance in-situ, if the degree of saturation is appropriately estimated.

To evaluate an augmentation in liquefaction resistance

[i] Department of Civil and Environmental Engineering, Ehime University, Japan (hide@dpc.ehime-u.ac.jp).
[ii] Chugoku Regional Development Bureau, Ministry of Land, Infrastructure, Transport and Tourism (formerly Graduate Student of Ehime University).
The manuscript for this paper was received for review on April 14, 2008; approved on October 3, 2008.
Written discussions on this paper should be submitted before July 1, 2009 to the Japanese Geotechnical Society, 4-38-2, Sengoku, Bunkyo-ku, Tokyo 112-0011, Japan. Upon request the closing date may be extended one month.

via soil desaturation by air injection in design practice, the rates, magnitudes, and distributions of the desaturation should be predicted, *a priori*. Model tests at 1 g (Reddy and Adams, 2001; Nishigaki et al., 2008) and in centrifuges (Marulanda et al., 2000; Ishihara et al., 2003; Okamura and Elgamal, 2006; Igarashi et al., 2008) as well as full-scale field experiment (Nishida et al., 2008) have been conducted to look into evaluation of desaturated zones. They identified the zones where soils are effectively desaturated by the air injection and showed that the area and distribution of degree of saturation are significantly influenced by soil type and soil stratification as well as air injection pressure and depth. This complicated nature clearly suggests a strong need for assistance of analytical methods for the prediction in design practice.

In the field of air-sparging for subsurface remediation, mathematical modelings and numerical simulations are popular to predict behavior of a multiphase flow within soils (Lundegard and Andersen, 1996; McCray, 2000; Tsai, 2007). Specifically, McCray (2000) reviewed the existing mathematical models describing the behavior moderated by air sparging and concluded that the multiphase flow models might be very useful to describe a desaturation process induced by air sparging as long as detailed model calibration is well-conducted. However, those studies focused on the remediation process from contaminated coarse materials instead of fine sand and silt, and have paid little attention to the degree of saturation in the desaturated zone.

In this study, desaturation experiments utilizing air-injection probes are conducted using the two different sizes of soil containers. The experiments with the small container are to examine the nominal rates and magnitudes of soil desaturation driven by air injection, whereas those with the large are to obtain not only the rates and magnitudes but also the distributions of the desaturated zones within the soil. We also attempt to predict the measured desaturation processes both during air injection and after the injection has halted, using a multiphase flow simulator for the both experiments and examine the validity of the simulator if it is capable of being applied to real sites.

## EXPERIMENTS

A desaturation process within soils via air injection is examined using the two different sizes of containers as shown in Fig. 1. The small container is relatively simple to conduct experiments–preparing model grounds is straightforward due to the smaller volume and an average degree of saturation is measured within a whole domain, but have a limitation that horizontal expansion of airflow may be interfered by side walls. The large container on the other hand has several advantages: sufficiently wide side-walls never hinder airflows, and local and temporal changes of degree of saturations are measured by TDR (Time Domain Reflectometry) probes inserted within the container. However, preparing model grounds is relatively laborious because of its bulk, and it has a potential against boiling sand as overburden pressure may not be applied equivalently on the top of grounds. Both experiments are explained in detail in the following sections.

### *Experimental Measurements with Small Container*

The small container (Fig. 1) is made of transparent acrylic boards with a internal dimension of 70 cm height, 25 cm width, and 10 cm depth. A fully saturated 27 cm-height model ground is constructed in such a way that dry Toyoura sand is rained in water and compacted every 5–8 cm height to have a relative density of 60% (i.e., a void ratio of 0.755). After construction, an effective overburden pressure of 50 kPa is applied on the top of the ground to prevent the soil from boiling and piping mediated by

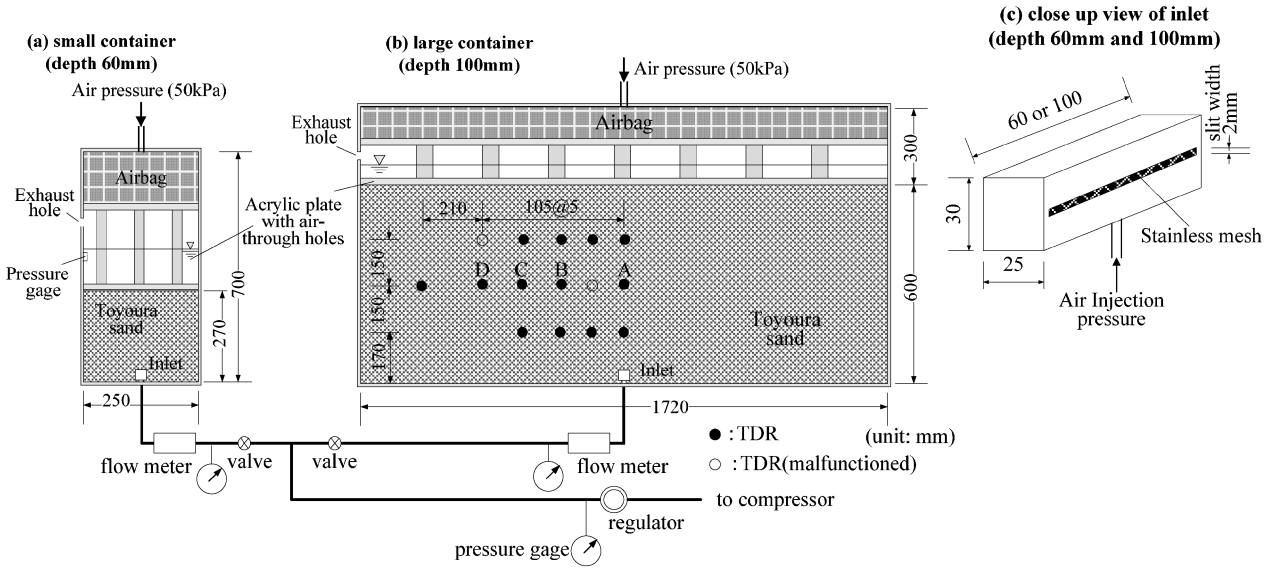


**Fig. 1. Schematic of the two experimental containers ((a) small and (b) large) and (c) focused view of the inlet for air injection: for the large one, local saturations are measured by TDR probes (presented by black circles) and additionally at the locations (A)–(D), temporal changes in saturation are continuously measured**

**Table 1. Experimental conditions using small container and soil properties modeled**

| Air pressure (net) [kPa] | Ground height [cm] | Relative density [%] | Porosity [−] |
|---|---|---|---|
| 8(4) | 26.3 | 48.4 | 0.443 |
| 10(6) | 29.0 | 64.0 | 0.425 |
| 13(9) | 27.4 | 60.6 | 0.429 |
| 8(4)→10(6)→13(9) | 27.8 | 67.4 | 0.421 |

air injection. A water pressure gage is installed above the model ground to continuously measure an evolution of the water level induced by air injection. Thus, an average degree of saturation, $S_r$, within the model ground may be simply evaluated with time, as,

$$S_r(t) = S_{r0} - \frac{\Delta h(t)}{h_s \cdot \phi}, \quad (1)$$

where $S_{r0}$ is the initial degree of saturation that is set to be 1.0 as a initial condition. $\Delta h(t)$ represents the change of water level from the initial with time. $h_s$ is the height of the model ground after consolidation, and $\phi$ is the porosity. Air is supplied into the ground through inlet ports located on the center-bottom of the both containers (Fig. 1). Representing 2-D condition in terms of airflow behavior, 2-mm-height mesh slits, rectangular in shape, are set on both sides of the inlets in the depth direction − 10 cm and 6 cm depth, equivalent to the container depth, in the small and large containers, respectively. Air pressures injected and airflow rates are measured by the flow meter installed in injection line close to, and right before the inlets (*see* Fig. 1).

A suit of air injection experiments are conducted at several air-pressure conditions as tabulated in Table 1–air pressures of 8, 10, and 13 kPa, higher than the air entry value (i.e., 4 kPa) adding hydrostatic pressure, are kept constant throughout the three individual cases and those are increased periodically from 8–13 kPa in the last case. Net air pressures, defined as differential between the gross air pressure and hydrostatic pressure at the inlet, are namely 4, 6, and 9 kPa. These are additionally shown for comparison to those in the large-container experiments.

Water retention characteristics of the sand was tested by the pressure plate method and the air entry value was found to be 4.0 kPa. In the preliminary tests using the small container, the air pressure was increased very gradually to look into the pressure at which air began to flow into the sand. The pressure was in a small range between 3.2 and 3.7 kPa higher than the hydrostatic pressure at the inlet, which is approximately consistent with the pressure plate test result.

Once injected, it is observed that air dominantly flows in horizontal direction, and moves upwards after reaching the side walls, which is enabled by a transparent container wall showing brighter colored soils induced by desaturation. This implicates that the horizontal permeability may be greater than the vertical. After a certain time (ca. 3000 sec in this work) as the airflow behavior (i.e., rate and degree of saturation) becomes steady,

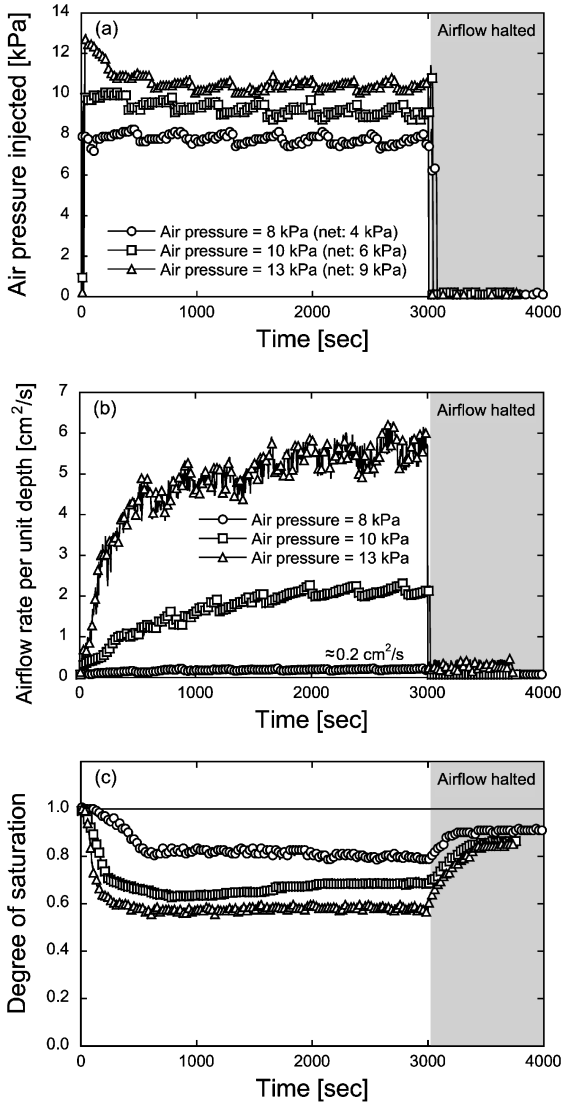


**Fig. 2. Changes in (a) air pressure injected (net air pressures are added as a reference), (b) airflow rate per unit depth and (c) degree of saturation with time for the small-container experiments**

the airflow is kept halted until buoyant air becomes stagnant and degree of saturation reaches the ultimate.

The evolutions of air pressure injected, airflow rate per unit depth (i.e., normalized in case for a two dimensional situation), and degree of saturation by air injection are depicted in Fig. 2. As apparent from Fig. 2(a), the air pressures measured adjacent to the inlet slightly oscillate. However, those are well-controlled throughout the experiments even though the uncertainties measured are explicitly involved. For the case of air pressure of 13 kPa, air pressure sharply decreased immediately after the air injection initiated. This may be attributed to the fact that air flow rate becomes significantly higher in this case right after the injection, incapable of supplying enough air by relatively thin tube used in the test to maintain the air pressure prescribed, which also occurs in the large-container experiments.

Airflow rates per unit depth measured also fluctuate corresponding to air pressure injected. They increase with

time and reach the steady values of 0.2, 2.0, and 5.5 $cm^2/s$ at the air pressures of 8, 10, and 13 (net: 4, 6, 9) kPa, respectively. Degree of saturation monotonically decreases with time down to those of 80, 67, and 58% at 8, 10, 13 (net: 4, 6, 9) kPa, respectively. After the temporal steady state, the air injection is halted. Subsequently, the degree of saturation gradually increases with time and recovers up to 85–90%, but never reaches the fully-saturated state due to residual air trapped within the pore spaces.

To validate reducibility and independency of desaturation process, the experiments under a periodically increased air pressure ranging 8–13 (net: 4–9) kPa, are conducted, and compared with those at independently prescribed pressures of 8, 10, and 13 (net: 4, 6, 9) kPa as shown in Fig. 3–the starting times for the experiments at 10 and 13 (net: 4, 9) kPa, are shifted to match with the timings of the air pressures increased. It shows significant agreement between those under different air pressurized conditions, indicating that rates and magnitudes of desaturation processes are dominantly controlled by air pressure subscribed. Moreover, the ultimate residual degree of saturation is 86%, congruent with those obtained from the experiments under other different conditions. This proves that ultimate magnitude of air volume trapped within a tributary volume after air supply ceases, are independent of the air pressure prescribed, and also implicates that the air pressure prescribed exerts influence over spatial ranges of desaturation, which is examined in the following section.

*Experimental Measurements with Large Container*

The large container (90 cm height × 172 cm width × 6 cm depth) is significantly wider than the small. Thus, airflow is not hindered by the side walls. Moreover, local degrees of saturation during experiments, are intermittently measured using TDR probes at the fifteen locations (two of them malfunctioned), and notably temporal evolution are also measured at the locations (A), (B), (C), and (D) (Fig. 1). TDR probes are arranged so that boundaries between desaturated and saturated zones are detected, rather than measuring distribution of degree of saturation in detail in desaturated zone.

All sensors were calibrated in uniform beds of Toyoura sand prepared in a calibration box at several densities and water contents. Linear relationships between volumetric water content and output signal voltage were successfully

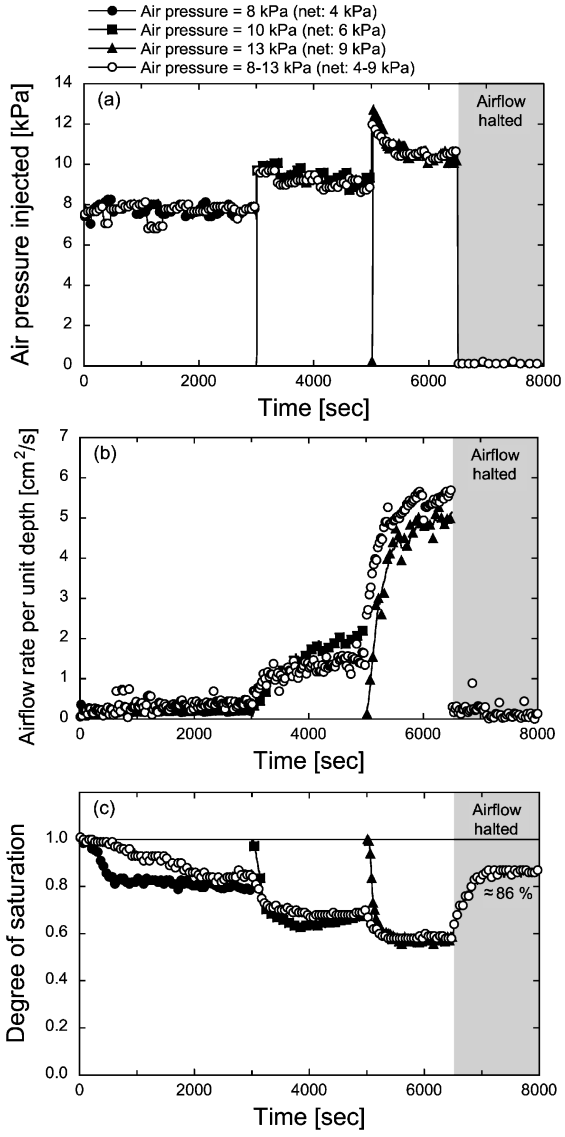


**Fig. 3. Changes in (a) air pressure injected, (b) airflow rate per unit depth and (c) degree of saturation with time for the small-container experiments under air pressured 8–13 kPa (i.e., net air pressure ranging 4–9 kPa)**

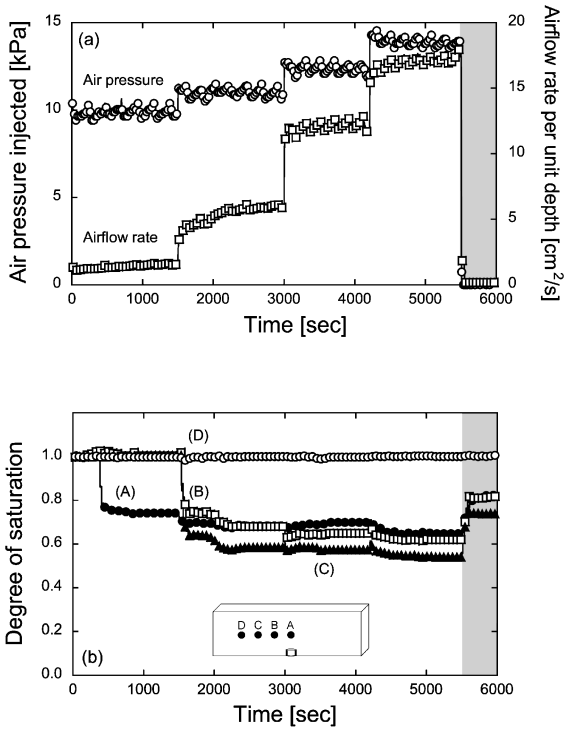


**Fig. 4. Changes in (a) air pressure injected and airflow rate per unit depth and (b) degree of saturation with time for the large-container experiments under air pressured 10–15 kPa (i.e., net air pressure ranging 3–8 kPa)**

established with correlation coefficients higher than 0.998.

The model ground is constructed in the same way as that for the small container, and the final height of the ground is 60 cm. This ground is also pressurized by an overburden pressure of 50 kPa. Experiments using the large container are conducted at periodically augmented air pressures ranging from 10–15 (net: approx. 3–8) kPa, and time-dependent evolutions and spatial distributions of degree of saturation are vigorously examined, which is succeeded by TDR probes.

Changes in air pressure, airflow rate per unit depth, and degree of saturation at the locations (A), (B), (C), and (D) are depicted in Fig. 4. As noted in the previous section, the large air pressures (i.e., 15 kPa in this case) may not be consistently prescribed due to high airflow rates observed, that is unlikely followed by the thin air-supply tube although the tube utilized is thicker than that used in the small-container experiments. This results in a gradual depression in the air pressures as also measured

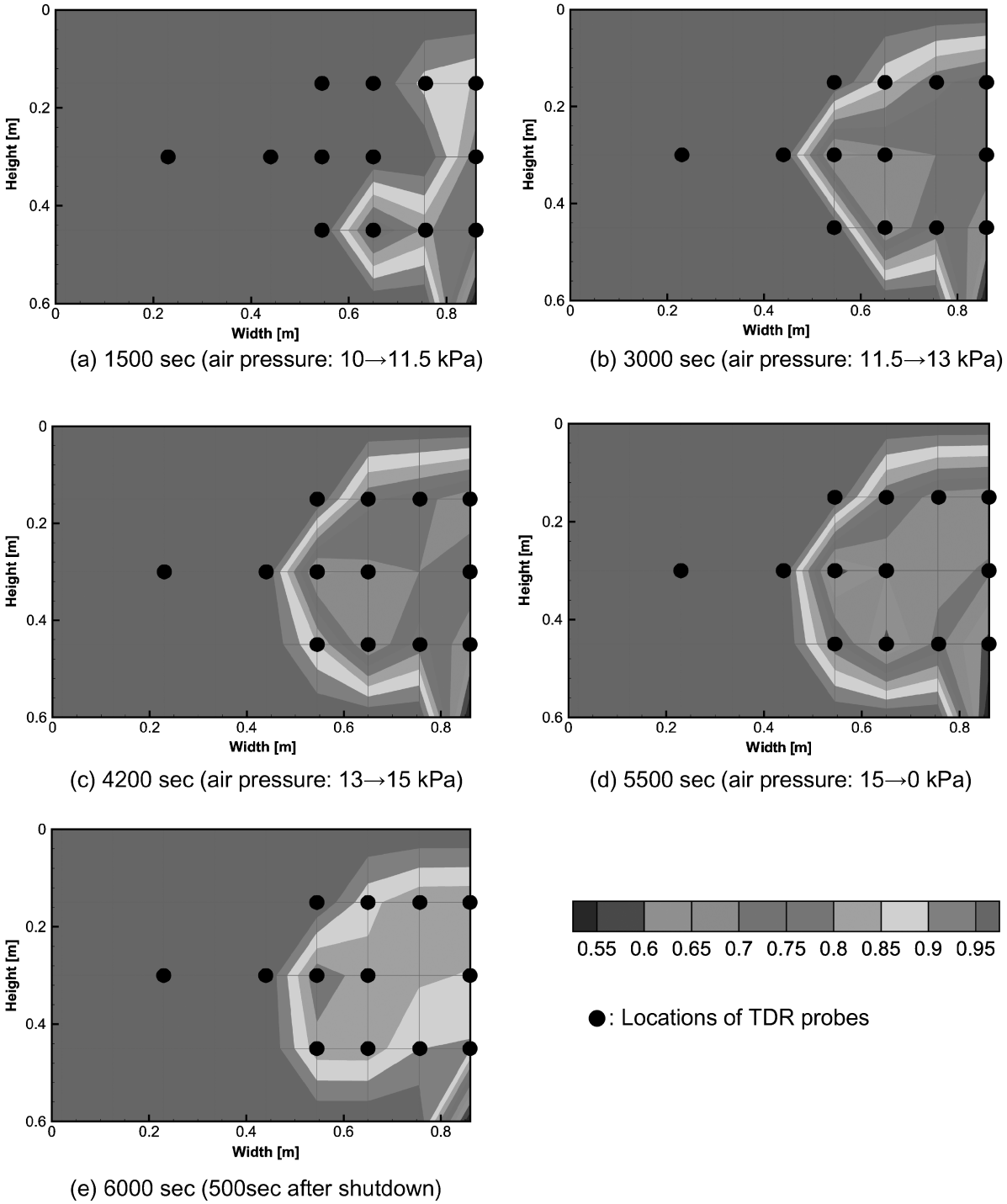


**Fig. 5. Distributions of saturation evaluated by TDR probes within the large-container ground at (a) 1500, (b) 3000, (c) 4200, (d) 5500 and (e) 6000 sec (note that one half domain is shown)**

in the small-container experiments in the case of 13 kPa (*see* Fig. 3). Airflow rate increases with increase in air pressure although the measured air pressures are slightly less than the prescribed as observed in the small-container experiments (Fig. 4(a)), whereas degrees of saturation at the locations (A), (B), and (C) following the sharp reductions down to roughly 60%, slightly evolves with time (Fig. 4(b)). Note that flow around the location (D) may be stagnant and the soil keeps fully-saturated throughout the experiments and as a result the airflow never reaches there. Once air injection is halted, the degrees of saturation at (A), (B), and (C) abruptly increase up to roughly 80%. The degree of saturation at (A) starts increasing earlier than at the locations (B) and (C), and this is merely attributed to the shorter distance from the airflow inlet.

An important component of this experimental system is the ability to continuously or intermittently measure the local distributions of degree of saturation within the soil ground. The local degree of saturations are evaluated by the thirteen TDR probes at the timings when an air pressure is newly prescribed and is halted. The deduced contour maps of degree of saturation based upon the locally and temporally evaluated, is depicted in Fig. 5. Note that the maps are created based on the three premises–1) Fifty lattice points are utilized where the thirteen TDR probes measured are located within the latticed mesh, 2) the degree of saturation at the right-bottom corner is assumed to be 0.5 times that on the periphery of the air injection inlet, and 3) those at all boundary points except the TDR measured and the right-bottom, are prescribed to be unity. As apparent in Fig. 5, the area desaturated increases with increase of the air pressure. It should be noticed that although degree of saturation increases by 2–5% when airflow is halted, the desaturated area little evolves even after air supply is ceased–we have neglected the model ground under a stagnant condition for about 60 days after the air halt, and then recognized little changes in the degree of saturation within the domain, which is congruent with the experimental measurements by Nishigaki et al. (2008). This indicates that desaturated area by air-injection is constrained when the distribution and magnitude of degree of saturation is well-predicted.

Experimental measurements with small and large containers show a desaturation process mediated by air injection to be followed with time (and space only for the large-container experiments). This well-presented results are attempted to be replicated by a multiphase flow predictions, that is explained in the following chapter.

## PREDICTIONS BY MULTIPHASE FLOW SIMULATION

Simultaneous flow of water and air occurs during air injection (i.e., desaturation process). Thus, the effects of capillary pressures and the mutual flow impedance between the two phases should be involved in the model with a theoretical assessment. In this chapter, firstly a suite of the mathematical equations used for the multiphase flow simulations is presented and then the parameters for predictions are identified through replicating the laboratory tests for determining soil-water retention characteristics. Finally, the comparison results between the experimental measurements and the predictions are shown in detail.

### *Mathematical Formation for Multiphase Fow*

We use a multiphase flow simulator of TOUGH2 (Pruess et al., 1999) to describe a desaturation process and to examine an applicability of the model if replicating the experimental measurements. TOUGH2 solves mass and energy balance equations that describe fluid and heat flow in general multiphase, multicomponent systems. In this code, space discretization is made directly from the integral form of the basic conservation equations, without converting them into partial differential equations. This ''integral finite difference'' method (IFDM; Edwards, 1972; Narasimhan and Witherspoon, 1976) avoids any reference to a global system of coordinates, and thus offers the advantage of regular or irregular discretizations in one, two, and three dimensions. Time is discretized fully implicitly as a first-order backward finite difference. This together with an upstream weighting of flux terms at interfaces is adopted to avoid impractical time step limitations in flow problems. Time steps are automatically adjusted (increased or reduced) during a simulation run, depending on the convergence rate of the iteration process. Automatic time step adjustment is essential for an efficient solution of multiphase flow problems, where intrinsic time scales for significant changes in the flow system may vary by many orders of magnitude during a simulation run.

In TOUGH2, a mass balance may be expressed in integral form for arbitrary sub-volume, $V_n$, bounded by a surface area of $\Gamma_n$, given as,

$$\frac{d}{dt}\int_{V_n} M^\kappa dV_n = \int_{\Gamma_n} \mathbf{F}^\kappa \cdot \mathbf{n} d\Gamma_n + \int_{V_n} q^\kappa dV_n, \tag{2}$$

where $\kappa$ denotes the component, $M^\kappa$ is the amount of component .$\kappa$ with a dimension of mass per volume, $\mathbf{F}^\kappa$ is the flux of component $\kappa$, $\mathbf{n}$ is the outward unit vector normal to the volume surface, $q^\kappa$ is the rate of generation of component .$\kappa$ within the volume.

The mass accumulation term for air and water is given by,

$$M^\kappa = \phi \sum_\beta S_\beta \rho_\beta X_\beta, \tag{3}$$

where $S_\beta$, $\rho_\beta$, and $X_\beta$ denote the degree of saturation, density, and mass fraction of phase $\beta$ (liquid or gaseous phase), respectively. The advective mass flux terms summed over the liquid and gaseous phases, as,

$$\mathbf{F}^\kappa = \sum_\beta X_\beta^\kappa \mathbf{F}_\beta. \tag{4}$$

Advective flow for each phase $\beta$ is defined by considering the driving forces of pressure and gravity according to a multiphase extension of Darcy's law, given as,

$$\mathbf{F}_\beta = \rho_\beta \mathbf{u}_\beta = -k \frac{k_{r\beta}\rho_\beta}{\mu_\beta}(\nabla P_\beta - \rho_\beta \mathbf{g}), \quad (5)$$

where $\mathbf{u}_\beta$ is the $\beta$ phase Darcy velocity, $k$ is the intrinsic permeability, $k_{r\beta}$ is the $\beta$ phase relative permeability, $\mu_\beta$ is the $\beta$ phase dynamic viscosity, $P_\beta$ is the $\beta$ phase pressure, and $\mathbf{g}$ is the gravitational acceleration vector. The hydraulic conductivity, $K$, is evaluated through a simple laboratory test, and the intrinsic permeability, $k$, is obtained by the following relation between $K$ and $k$, given as,

$$k = \frac{\nu_w}{g} K, \quad (6)$$

The Mualem-van Genuchten model (Mualem, 1976; van Genuchten, 1980) is used to describe the relation between degree of saturation and $\beta$ phase relative permeability, as,

$$k_{rl} = \begin{cases} \sqrt{S^*}\,\{1-(1-[S^*]^{1/\lambda})^\lambda\}^2 & \text{if } S_l < S_{ls} \\ 1 & \text{if } S_l < S_{ls}, \end{cases} \quad (7)$$

$$k_{rg} = \begin{cases} 1 - k_{rl} & \text{if } S_l < S_{ls} \\ (1-\hat{S})^2(1-\hat{S}^2) & \text{if } S_l < S_{ls}, \end{cases} \quad (8)$$

where,

$$S^* = (S_l - S_{lr})/(S_{ls} - S_{lr}), \quad (9)$$

$$\hat{S} = (S_l - S_{lr})/(1 - S_{lr} - S_{gr}), \quad (10)$$

Here, $S_{ls}$ is the maximum liquid degree of saturation, and $\lambda$ is the constant. $S_{lr}$ and $S_{gr}$ denote the residual liquid and gaseous degree of saturation, respectively.

The relation between liquid ($l$) and gaseous ($g$) pressures is defined, via the capillary pressure, $P_{cap}$, as,

$$P_l = P_g + P_{cap}. \quad (11)$$

The relation between the capillary pressure and degree of saturation (i.e., water retention curve) may be described by the van Gennuchten equation (van Gennuchten, 1980), as,

$$P_{cap} = -P_0([S^*]^{-1/\lambda} - 1)^{1-\lambda}, \quad (12)$$

where $P_0$ is the constant that may be related to an air entry value.

The continuum equations (Eq. (2)) are discretized in space to numerically solve multiphase flow processes. After discretization as a first-order finite difference, the flux and sink and source terms are evaluated at the next time step. An iterative procedure is adopted to solve in time until a prescribed time.

*Constraining Retention and Permeability Functions*

The relation between the capillary pressure and degree of saturation (Eq. (12)) for the Toyoura sand utilized for the air injection experiments with the small and large containers, is determined through soil water retention experiments measured in this study and by Uno et al. (1998) as shown in Fig. 6, together with the well-fitted predictions by Eq. (12). The parameters used for the fitting is tabulated in Table 2. Uno et al. (1998) have utilized the Toyoura-sand specimens with the void ratio of 0.739, comparable to that of 0.755 for the model ground in the small- and large-container experiments. The relation between the capillary pressure and degree of saturation may little change between those two values of void ratio, implicating that a reliable fit by Eq. (12) is obtained using the both measurements.

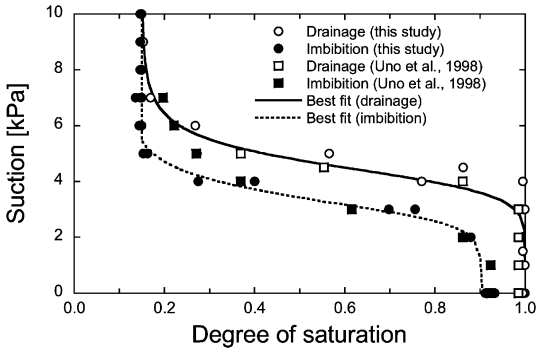


**Fig. 6. Replicating experimental measurements of water retention curves for drainage and imbibition processes**

**Table 2. Parameters used to fit water retention curve measured (Eqs. (7)–(12))**

| Parameters | Drainage | Imbibition |
|---|---|---|
| $\lambda$ | 0.885 | 0.856 |
| $P_0$ [kPa] | 4.47 | 3.31 |
| $S_{lr}$ | 0.155 | 0.145 |
| $S_{ls}$ | 1.00 | 0.901 |
| $S_{gr}$ | $1.00\times10^{-2}$ | $9.90\times10^{-3}$ |

The parameters of $\lambda$, $S_{lr}$, and $S_{ls}$ for relative permeability function (Eqs. (7)–(10)) are assumed equivalent to those determined from fitting the water retention curve for drainage. The residual gaseous degree of saturation of $S_{gr}$ is obtained from trapped air saturation at the end of the water retention experiment for imbibition (Table 2). The relation of relative permeability between liquid and gaseous phases with the determined values, is depicted in Fig. 7–for reference, the results from the literature (Uno et al., 1990, 1993; Sugii et al., 2002) are also shown.

The hydraulic conductivity is measured from constant head flow-through tests, and the obtained values are $2.0 \pm 0.5\times10^{-4}$ m/s, congruent with those obtained from Kohno and Nishigaki (1982). Therefore, the equivalent intrinsic permeability used for replicating the small- and large-container experiments is $2.04\times10^{-11}$ m$^2$.

*Comparison between Measurements and Predictions*

In small-container predictions, the dimension of the simulated model ground used in the analyses is 27 cm height × 25 cm width × 10 cm depth, equivalent to that in the small-container experiments, and the initial degree of saturation within the whole domain is set to be fully saturated. Air pressure exerted at the top elements is fixed to be 101.3 kPa of an atmospheric pressure. No flow conditions are prescribed at the boundaries of the bottom and

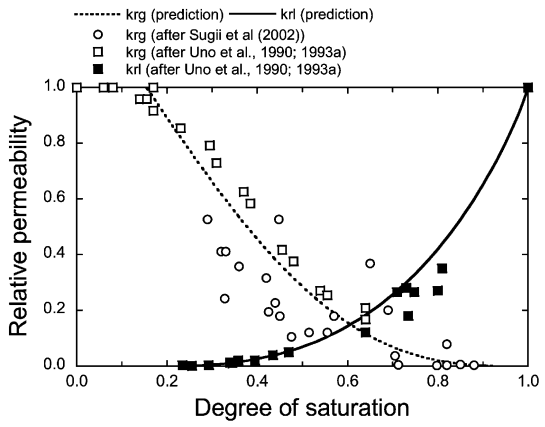


**Fig. 7. Relative permeability for liquid and gaseous phases determined from the predictions of water retention curves, together with measurements obtained from the literature (Sugii et al., 2002; Uno et al., 1990, 1993)**

the both right and left sides. Flow of air and water is allowed at the top boundary. A center-bottom element is chosen as an injection inlet with interfacial areas of 360 $mm^2$, equivalent to the slit size used in the experiments. Firstly, desaturation processes for the small-container experiments are predicted by the model previously described. Predictions of the evolution in degree of saturation and airflow rates per unit depth with the used parameters tabulated in Table 2, are shown in Fig. 8, together with the experimental measurements. Note that the air pressures prescribed for predictions are not the nominal values (i.e., 8, 10, 13 (net: 4, 6, 9) kPa in the small-container experiments) but the actual measurements observed by the flow meter installed as shown in Fig. 1, because the measured values become slightly lower than the initial prescribed values as indicated in the previous chapter. Generically, the horizontal permeability is thought to be greater than the vertical (Lambe and Whitman, 1979) although the horizontal is undefined in this study. Thus, predictions with the three- and five-fold horizontal permeability based on the vertical values, are also conducted and depicted in Fig. 8. Focused on airflow rates, predictions slightly overestimate, but show relatively good agreement with, the actual measurements for all air pressure conditions. Notably, airflow rates increase with increase of horizontal permeability, which is due to augmentation of nominal permeability (i.e., a sum of vertical and horizontal effects).

Predictions of the degree of saturation are fairly situated within the measurements and show slight differences between those with one-, three-, and five-fold horizontal permeabilities. This underestimation may be attributed to the higher flow rates predicted. Also note that the residual degrees of saturation predicted are equivalent to those obtained by the experiments under all conditions. This is the most important output for this simulation because for the air-injection technique proposed by Okamura and Teraoka (2005), temporal and spatial magnitude desaturated must be predicted prior to its execution in a field. Predictions for the small-container experiments clearly show a validity of the model to understand the temporal changes of degree of saturation in a whole tributary domain.

In large-container predictions, the domain is congruent with the model ground constructed in the experiments. Initial and boundary conditions prescribed are set by following the same procedure explained in the small-container predictions. Predictions of desaturation processes in a large container are aimed to examine the viability if they are locally and temporally capable of describing the experimental measurements. Figure 9 shows the air pressure used for the predictions as boundary conditions in the large-container experiments. Predictions in the airflow rates (Fig. 9) underestimate the measurements–roughly 10 to 70% smaller than the actual although the higher the air pressure and the horizontal permeability, the smaller the mismatch. Predictions of the degree of saturation with one-, three-, and five-fold horizontal permeabilities are shown in Fig. 10. Predictions indicate that air reaches the location (D), which is incongruent with the measurements. However, for other locations (A), (B), and (C) predictions approach the actual as air pressures prescribed increase. Notably, predictions in the locations (A) and (B) well follow the measured at the air pressure of 15 (net: 8) kPa. As predicted for the small-container experiments, the residual degrees of saturation are well-predicted under all permeability conditions. The mismatch of degree of saturation may be attributed to the underestimation of the flow rates predicted in resulting from that physical properties (e.g., intrinsic and relative permeability, and drainage and imbibition characteristics) of the soil ground may not be well-replicated from those obtained from the theoretical manner (Eqs. (7)–(10)) and the water retention experiments. In other words, those properties should be examined and identified, in advance, before conducting predictions in fields.

Figure 11 shows comparison of the relation between net air pressures (i.e., differential between nominal air pressure prescribed and hydrostatic pressure at the bottom of the containers) and airflow rates per unit depth. In the small container, the airflow rates predicted shows a good agreement with the measurements, and show a linear tendency with increase of the net air pressure. Note that this tendency is also indicative in the large-container experiments and predictions, but the observed values in the experiments are greater than those predicted. This is due likely to soils more permeable in the large container, which has no accounted effect in predictions (i.e., the same permeability utilized in the both small- and large-container predictions).

Evolution of local distributions of degree of saturation is predicted in case that $K_h = K_v$ as shown in Fig. 12, compared with the experimentally evaluated (Fig. 5). It is noticeable that the magnitude and distribution of desaturated soils at all timings are well-replicated by the predictions although these overestimate as time passes. Moreover, residual desaturated areas are also, though slightly overestimated, described by the simulated results.

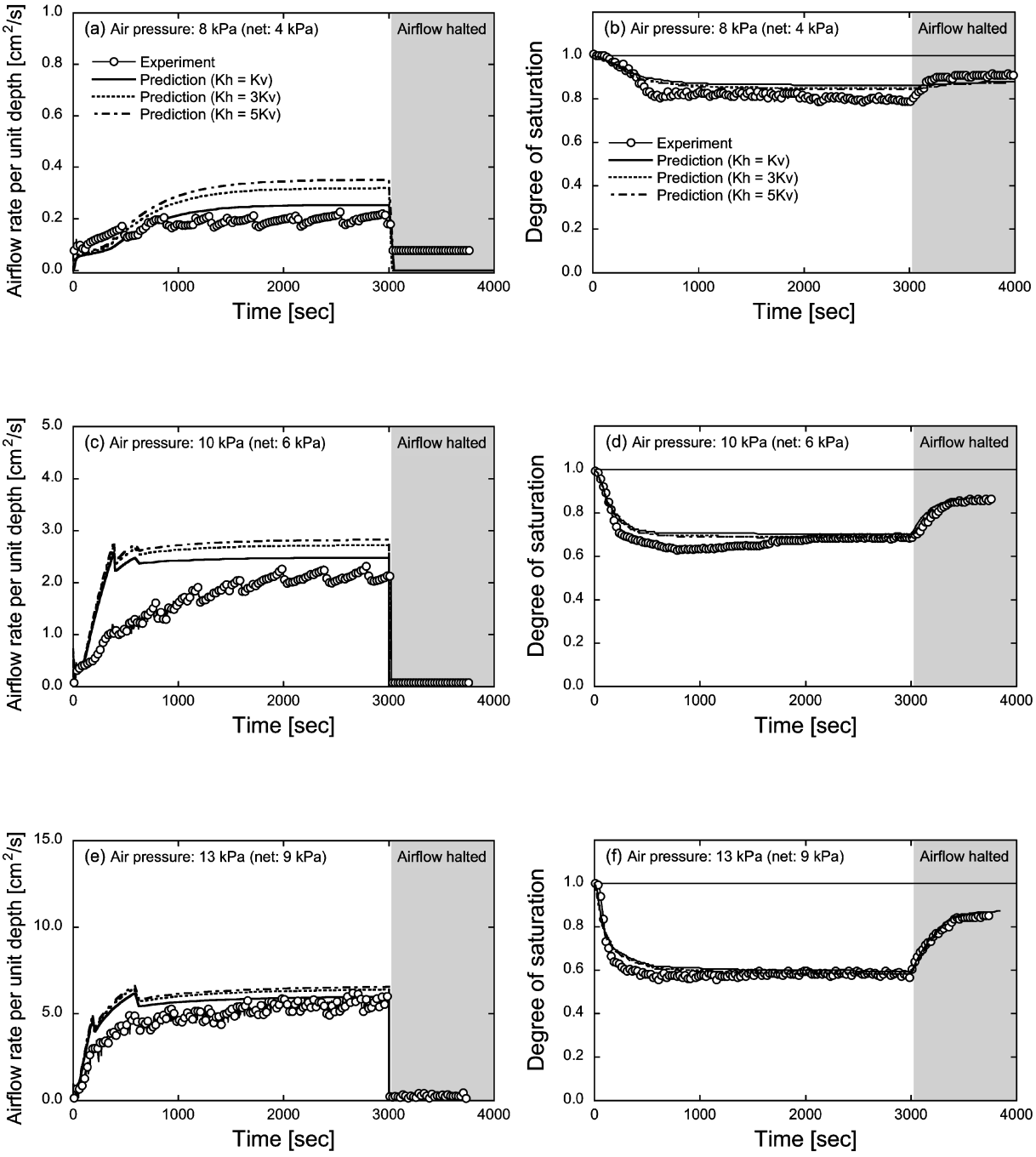


**Fig. 8. Comparisons of airflow rate per unit depth and degree of saturation between measurements and predictions at air pressures of 8, 10, 13 kPa (i.e., net air pressures of 4, 6, 9 kPa)**

This indicates that the model may be capable of predicting desaturation processes mediated by air injection under arbitrary conditions, and be applicable to field problems as flow characteristics are identified, *a priori*.

## IMPLICATIONS

In the last chapter, the model validity is vigorously examined by comparison between the predictions and the experimental measurements. The implications of this desaturation behavior may be examined by comparison with the reference behavior where the hydraulic conductivities (or intrinsic permeabilities), prescribed net air pressures, and the nature of permeability in horizontal and vertical directions and of desaturation process ($\lambda$ and $P_0$ in Eq. (12)), are changed, specifically to examine their anticipated effect on the evolution of desaturation processes. A fully-saturated domain is addressed as an initial condition, and the domain dimension used for the analysis is 10 m height $\times$ 40 m width $\times$ 0.1 m depth, with a water table equi-height to the domain surface.

Predicted results of the desaturated zones in steady state are summarized in Fig. 13, and the boundary conditions and modification of parameters used in this analysis

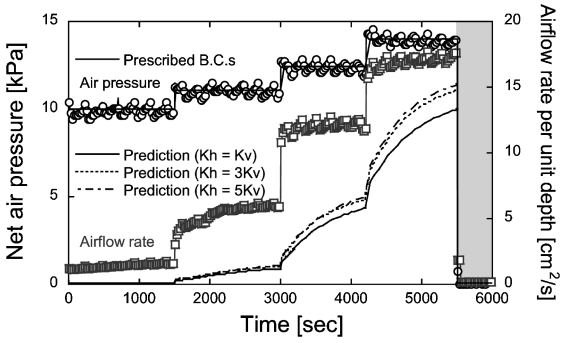


**Fig. 9. Air pressures prescribed for predictions and comparison of airflow rate per unit depth between measurements and predictions with one-, three-, and five-fold horizontal permeability against vertical value**

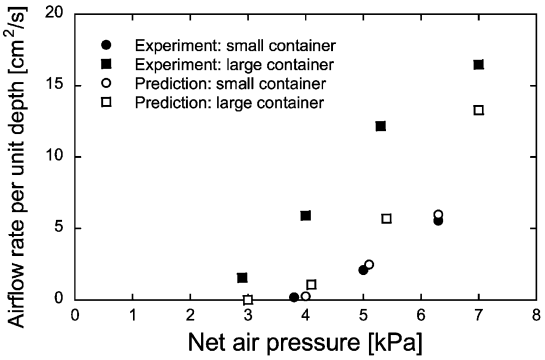


**Fig. 11. Comparison of net air pressure and airflow rate per unit depth in steady state between measurements and predictions in case that $K_h = K_v$**

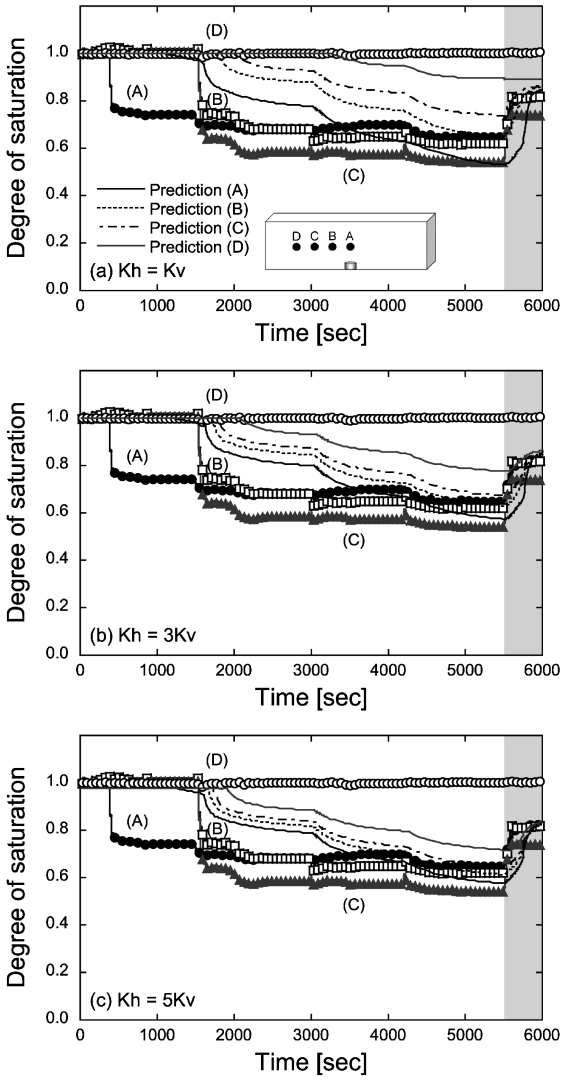


**Fig. 10. Comparisons of degree of saturation between measurements and predictions with one-, three-, and five-fold horizontal permeability against vertical value**

are tabulated in Table 3. Those with the hydraulic conductivity (or intrinsic permeability) changed (the first row in Fig. 13) show no difference in magnitudes of the desaturated areas among the three cases. However, the airflow rates per unit depth predicted, linearly increase with increase of the hydraulic permeability $-13.3$, $1.33 \times 10^2$, and $1.33 \times 10^3$ cm$^2$/s with $K = 3.0 \times 10^{-6}$, $3.0 \times 10^{-5}$, and $3.0 \times 10^{-4}$ m/s, respectively. Likewise, the durations to reach steady state are inversely proportional to the conductivity, ranging from $1.5 \times 10^5$–$1.5 \times 10^7$ [sec]. This is attributed to the constant air pressure fixed, concluding that soil permeability merely controls rates of the desaturation behavior with linear effects and not for magnitudes and distributions where the horizontal and vertical permeabilities are identical.

Predictions with the net air pressures varied (the second row in Fig. 13) clarify that desaturated zone in steady state increases with increase of the air pressure–the maximum desaturated width (i.e., top-width of mortar-like desaturated zones in the figures) augments by a factor of two as it is changed from 20 to 80 kPa. Airflow rates per unit depth predicted, as expected, also increase with increase of the net air pressure with the values of $5.83 \times 10^2$, $1.33 \times 10^3$, and $1.95 \times 10^3$ cm$^2$/s at 20, 50, and 80 kPa, respectively, but this augmentation is not drastic as predicted in the case of permeability alternation.

Predictions with alternation of the horizontal permeability against the vertical fixed (the third row in Fig. 13) indicate that the desaturated increases with increase of the ratio of $K_h/K_v$. The maximum desaturated width linearly increases from 16 m to 36 m. This is due to the increase in an apparent whole permeability and airflow rates induced, implicating that for application to field problems, both the horizontal and vertical permeability should be identified to predict the maximum desaturated zones.

Finally, desaturation behavior is examined by changing the nature of desaturation process (i.e., a water retention curve), focusing on the two controlling parameters of $\lambda$ and $P_0$ in Eq. (12) (the forth and last rows in Fig. 13). Water retention curves utilized in the analysis with the two parameters modified are depicted in Fig. 14. Predictions for the parameter of $\lambda$ changes show that smaller the amount, the wider the maximum desaturated zone in steady state. This is attributed to the significant effect of

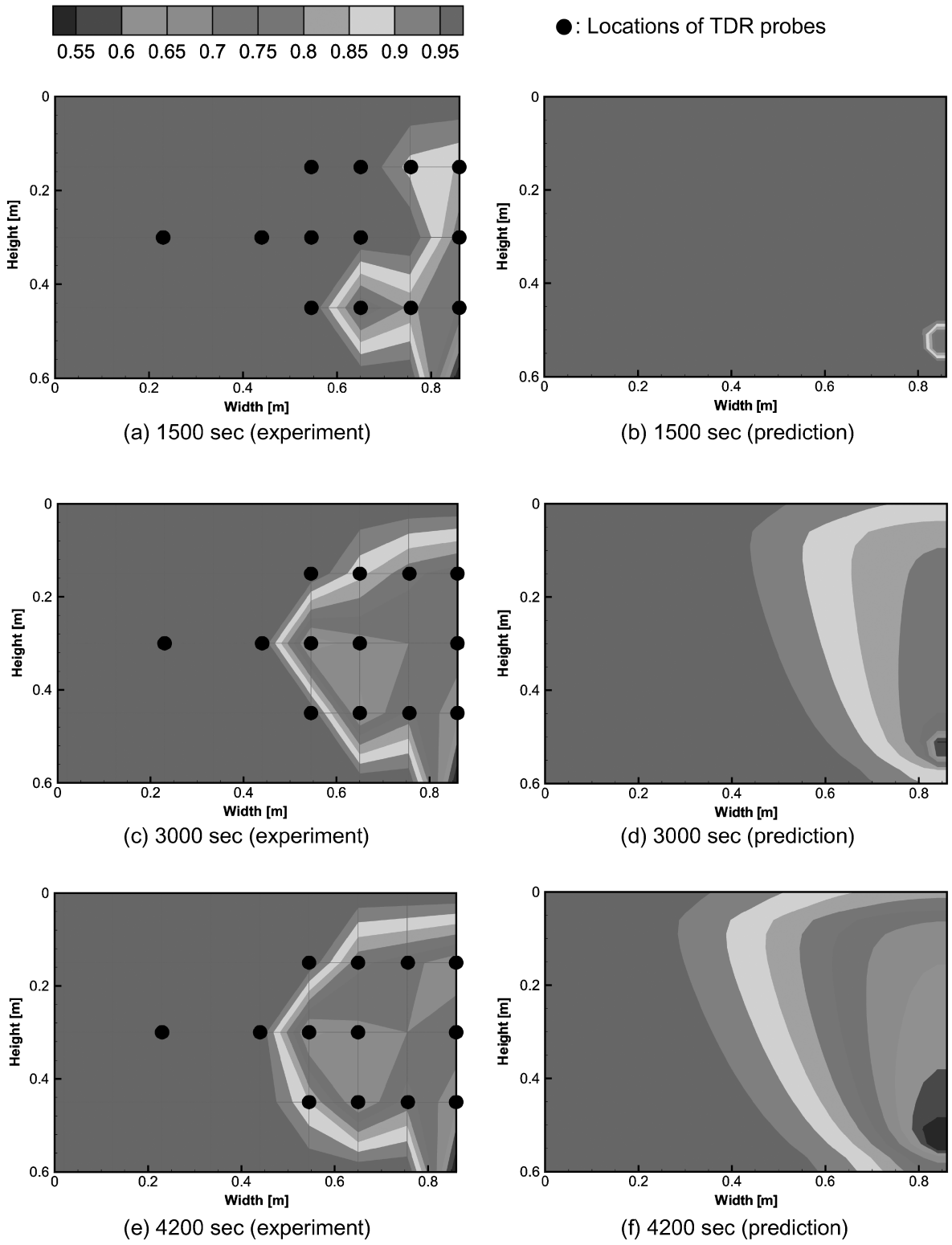


**Fig. 12. Comparisons of magnitude and distribution of desaturated zones between measurements and predictions in case that $K_h = K_v$**

suction exerted–the greater suction to make saturation reduced is required in a smaller $\lambda$, and thus the effect of buoyancy against suction becomes weaker, with the result that the air injected tends to transport more in the horizontal direction. Those for the parameter of $P_0$ changes indicate that greater the $P_0$, the narrower the maximum desaturated width because the differential between the air pressure prescribed and air entry value is smaller, and then airflow rates also decrease.

The implications mediated by predictions with several boundary conditions and the nature of soils changed, conclude that in order to obtain reliable estimations, characteristics of the flow transport for the soils targeted have to be examined and revealed in a laboratory, prior

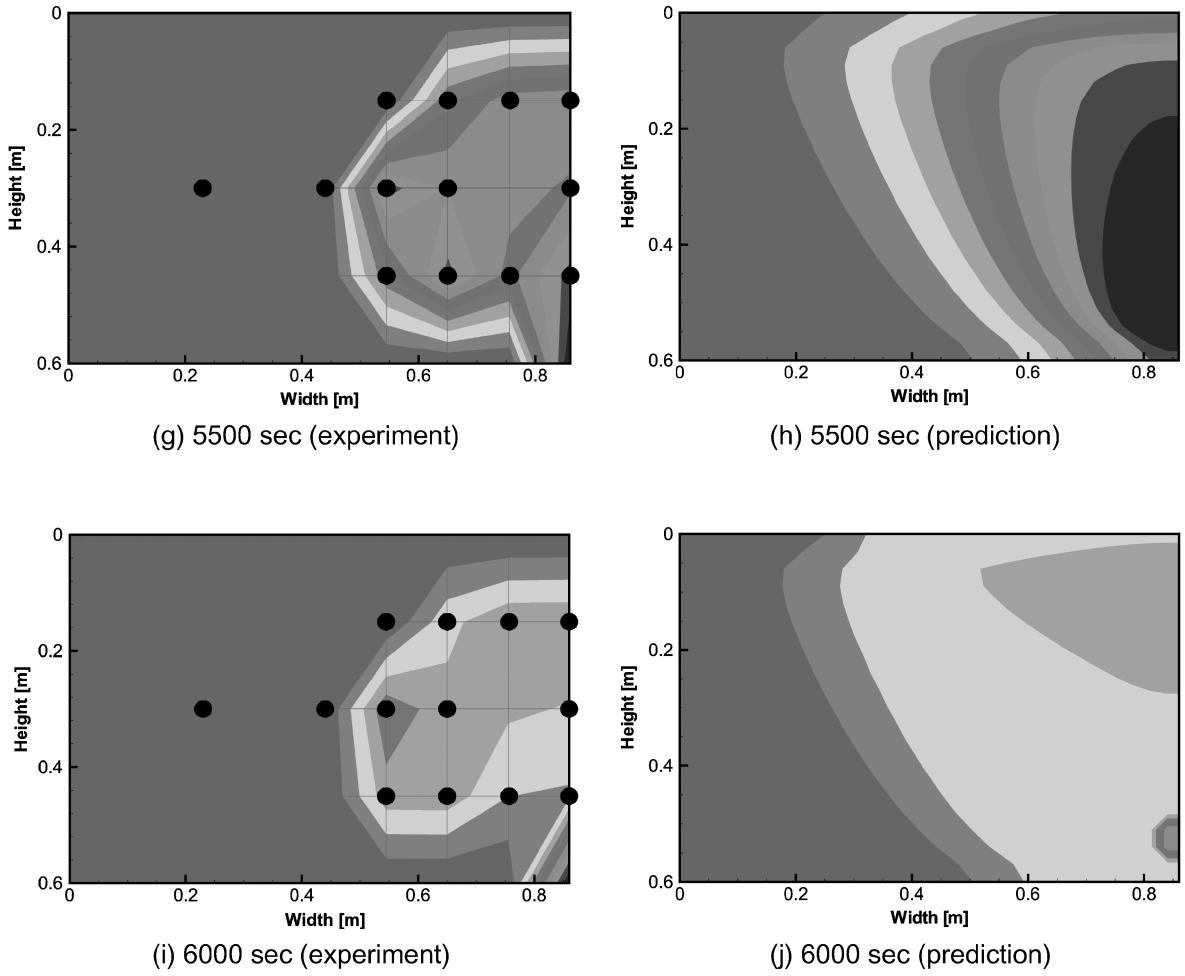


**Fig. 12. (continue)**

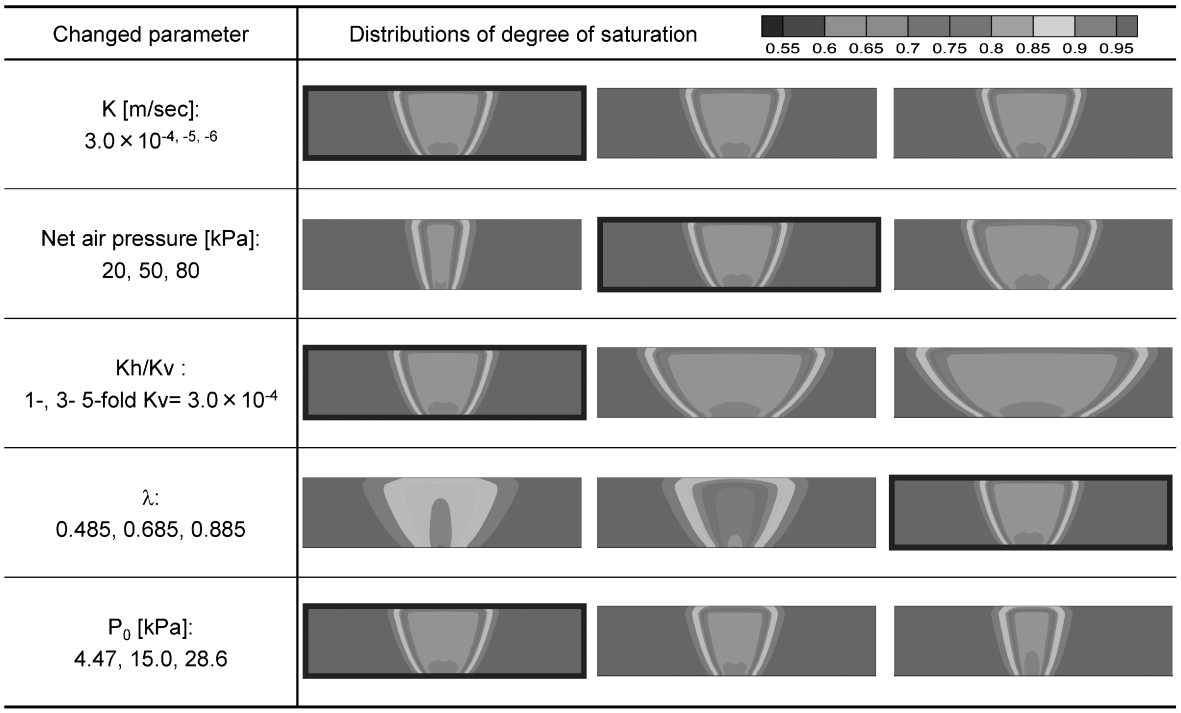


**Fig. 13. Distributions of steady-state saturation with various parameters changed for implication: black-surrounded are predictions as a reference under the conditions that $K_h = K_v = 3.0 \times 10^{-4}$ [m/s], $P_{air} = 50$ [kPa], $\lambda = 0.885$, and $P_0 = 4.47$ [kPa], and three figures in each row are the predictions with the three different values changed for the targeted parameter based on the reference**

**Table 3. Boundary conditions and modification of parameters used in the analysis**

| Parameters | $K$ [m/s] | Net air pressure [kPa] | $\lambda$ in Eq. (12) | $P_0$ in Eq. (12) |
|---|---|---|---|---|
| $K$ [m/s] | $3.0\times10^{-4,\,-5,\,-6}$ | 50 | 0.885 | 4.47 |
| Net air pressure [kPa] | $3.0\times10^{-4}$ | 20, 50, 80 | 0.885 | 4.47 |
| $K_h/K_v$ | 1-, 3-, 5-fold $K_v=3.0\times10^{-4}$ | 50 | 0.885 | 4.47 |
| $\lambda$ in Eq. (12) | $3.0\times10^{-4}$ | 50 | 0.485, 0.685, 0.885 | 4.47 |
| $P_0$ in Eq. (12) | $3.0\times10^{-4}$ | 50 | 0.885 | 4.47, 15.0, 28.6 |

* Grayed represent the focused and changed parameters for implications with the others fixed. Note that a reference condition is that $K_h=K_v=3.0\times10^{-4}$ [m/s], $P_{air}=50$ [kPa], $\lambda=0.885$, and $P_0=4.47$ [kPa].

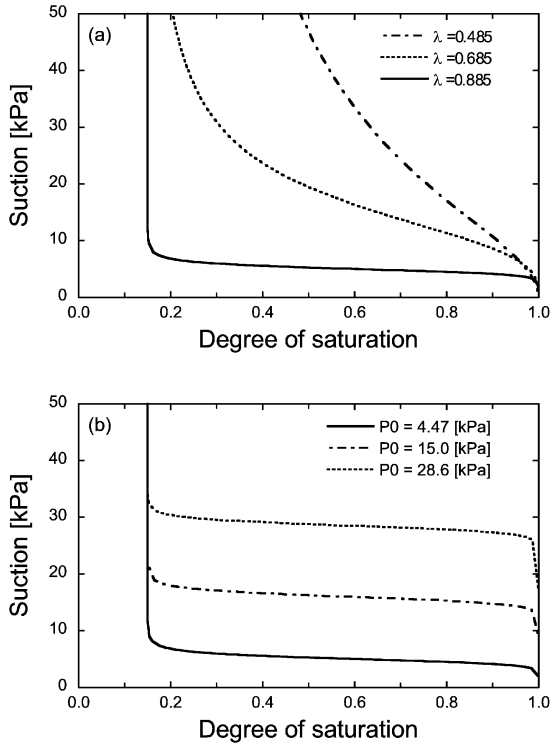


**Fig. 14. Water retention curves used in the implication analysis with modification of (a) $\lambda$ and (b) $P_0$**

to actually performing this air-injection in fields.

## CONCLUSIONS

This work experimentally and numerically examines the evolution in desaturation in terms of the rates, magnitudes, and distributions influenced by air injection. The two different sizes of ground containers are adopted–the small-container experiments are conducted to investigate overall desaturation process, whereas those with the large container enable local desaturation behavior to be followed with time using TDR probes.

In the small-container experiments at air pressures of 8, 10, and 13 (net: 4, 6, 9) kPa, the degrees of saturation monotonically decrease down to 88, 67, and 60%, respectively, within a relative short time, followed by a steady state. After a shutdown of the airflow, the degrees of saturation recover to the maximum liquid degree of saturation for imbibition (i.e., approx. 85%), and never reach a fully-saturated degree due to air trapped within pore spaces.

In the large-container experiments local degrees of saturation are evaluated by TDR probes and show that after sharp reductions down to roughly 60% at the locations (A), (B), and (C) those degrees of saturation stay steady although the airflow rates increase with increase in the air pressures. When the airflow is halted, the degrees of saturation abruptly increase to 80%, congruent with the results in the small-container experiments.

Numerical simulations by a multiphase flow model show good agreements with the experimental measurements of the evolution in degrees of saturation and airflow rates for the small-container experiments. Although mismatch on the rates and magnitudes of desaturation during air injection is observed in the large container, predictions well-replicate desaturated degrees for residual situation after air-injection had ceased. The whole simulation results conclude that this model may be applicable to predict desaturation processes in situ to be followed with time and space as flow characteristics are identified.

The implications obtained by changing intrinsic permeability, air-injection pressures, and the nature of permeability in horizontal and vertical directions and of water retention, reveal that when the air-injection technique is applied to real fields, laboratory experiments to understand characteristics of the flow transport should be carefully conducted to estimate desaturation behavior with sufficient precision and accuracy.

## ACKNOWLEDGEMENTS

This work has been partly supported by the Grant-in-Aid for Scientific Research (No.17360227) from the Ministry of Education, Sports, Science and Technology, Japan. This support is gratefully acknowledged.

## REFERENCES

1) Edwards, A. L. (1972): TRUMP: A computer program for transient and steady state temperature distributions in multidimensional systems, *National Technical Information Service, National Bureau of Standards*, Springfield, VA.
2) Ishihara, M., Okamura, M. and Oshita, T. (2003): Desaturating sand deposit by air injection for reducing liquefaction potential, *Proc. 2003 Pacific Conf. Earthquake Eng.*, Paper No. 89, CD-ROM.
3) Kohno, I. and Nishigaki, M. (1982): Some aspects of laboratory permeability test, *Soils and Foundations*, **22**(4), 181–180.
4) Lambe, T. W. and Whitman, R. V. (1979): *Soil Mechanics, SI Ver-*

*sion*, John Wiley and Sons, New York, 266–280.
5) Lundegard, P. D. and Andersen, G. (1996): Multiphase numerical simulation of air sparging performance, *Ground Water*, **34**, 451–460.
6) McCray, J. E. (2000): Mathematical modeling of air sparging for subsurface remediation: state of the art, *J. hazard. Mater.*, **72**, 237–263.
7) Mualem, Y. (1976): A new model for predicting the hydraulic conductivity of unsaturated porous media, *Water Resour. Res.*, **12**, 512–522.
8) Narasimhan, T. N. and Witherspoon, P. A. (1976): An integrated finite difference method for analyzing fluid flow in porous media, *Water Resour. Res.*, **12**(1), 57–64.
9) Nishida, K., Takebayashi, M., Fujii, N. and Okamura, M. (2008): In-situ test on soil desaturation bu air injection method–Part 1: Outline of the test, *Proc. 43rd Ann. Conf. Japanese Geotech. Soc.*, CD-ROM (in Japanese).
10) Okamura, M. and Teraoka, T. (2005): Shaking table tests to investigate soil desaturation as a liquefaction countermeasure, *ASCE Geotechnical Special Publication*, **145**, 282–293.
11) Okamura, M. and Elgamal, A. (2006): Centrifuge tests on desaturation of silt by air injection, *Proc. 61st Ann. Meeting of JSCE*, CD-ROM (in Japanese).
12) Okamura, M. and Soga, Y. (2006): Effect on liquefaction resistance of volumetric strain of pore fluid, *Soils and Foundations*, **46**(6), 703–708.
13) Pruess, K., Oldenburg, C. and Moridis, G. (1999): *TOUGH2 User's Guide Version 2.0*, Rep. LBNL–43134, Berkeley, CA, 197pp.
14) Reddy, K. R. and Adams, J. A. (2001): Effects of soil heterogeneity on airflow patterns and hydrocarbon removal during in situ air sparging, *J. Geotechnical and Geoenvironmental Eng.*, ASCE, **127**(3), 234–247.
15) Sugii, T., Yamada, K. and Yogo, T. (2002): Study on air permeability test for unsaturated soils, *Proc. 37th Ann. Conf. Japanese Geotech. Soc.*, 1275–1276.
16) Takemura, J., Seki, S., Igarashi, R. and Okamura, M. (2008): Centrifuge model tests of air injection in saturated sand, *Proc. 43rd Ann. Conf. Japanese Geotech. Soc.*, CD-ROM (in Japanese).
17) Takemura, J., Okamura, M., Igarashi, R., Masuda, M. and Izawa, J. (2009): Centrifuge model tests on soil desaturation as a liquefaction countermeasure, *Proc. 17 ICSMGE*, Alexandria (in press).
18) Tsai, Y. J. (2007): Airflow paths and porosity/permeability change in a saturated zone during in situ air sparging, *J. hazard. Mater.*, **142**, 3157–323.
19) Uno, T., Sato, T. Sugii, T. and Tsuge, H. (1990): Method of test for permeability of unsaturated sandy soil with controlled air pressure, *JSCE, J. Geotech. Eng.*, 618/III-13, 115–124 (in Japanese).
20) Uno, T., Kamiya, K. and Sugii, T. (1993): Considerations of the flow of air through soils based on the capillary model, *Proc. 37th Japan National Conf. Geotech. Eng.*, 25–32 (in Japanese).
21) Uno, T., Kamiya, K. and Tanaka, K. (1998): The distribution of sand void diameter by air intrusion method and moisture characteristic curve method, *JSCE, J. Geotech. Eng.*, 603/III-44, 35–44 (in Japanese).
22) van Genuchten, M. Th. (1980): A closed-form equation for predicting the hydraulic conductivity of unsaturated soils, *Soil Sci. Soc.*, **44**, 892–898.
23) Yegian, M., Eseller-Bayat, E., Alshawabkeh, A. and Ali, S. (2007): Induced-partial saturation for liquefaction mitigation: experimental investigation, *J. Geotechnical and Geoenvironmental Eng.*, ASCE, **133**(4), 372–380.
24) Yoshimi, Y., Tanaka, K. and Tokimatsu, K. (1989): Liquefaction resistance of a partially saturated sand, *Soils and Foundations*, **29**(3), 157–162.